Water Resources Research

RESEARCH ARTICLE

10.1029/2024WR037176

Uniting Surface Properties With Hydrodynamic Roughness in Shallow Overland Flow Models

Octavia Crompton[1,2], **Gabriel Katul**[2], **and Sally E. Thompson**[3]

[1]USDA ARS Hydrology and Remote Sensing Lab, Beltsville, MD, USA, [2]Department of Civil and Environmental Engineering, Duke University, Durham, NC, USA, [3]Department of Civil and Environmental Engineering, University of Western Australia, Perth, WA, Australia

Key Points:

- A runoff model is calibrated to 112 rainfall simulator experiments, and the results are used to compare four commonly used roughness schemes
- A transitional flow equation provides the best fit to the plurality of experiments
- Litter cover is the best predictor of roughness coefficients, followed by soil cover and average canopy gap size

Supporting Information:

Supporting Information may be found in the online version of this article.

Correspondence to:

O. Crompton,
octavia.crompton@usda.gov

Citation:

Crompton, O., Katul, G., & Thompson, S. E. (2025). Uniting surface properties with hydrodynamic roughness in shallow overland flow models. *Water Resources Research*, *61*, e2024WR037176. https://doi.org/10.1029/2024WR037176

Received 12 FEB 2024
Accepted 17 DEC 2024

Author Contributions:

Conceptualization: Octavia Crompton, Gabriel Katul, Sally E. Thompson
Formal analysis: Octavia Crompton
Investigation: Octavia Crompton
Methodology: Octavia Crompton, Gabriel Katul
Software: Octavia Crompton
Visualization: Octavia Crompton
Writing – original draft: Octavia Crompton
Writing – review & editing: Octavia Crompton, Gabriel Katul, Sally E. Thompson

Abstract

Describing flow resistance from the properties of an underlying surface is a challenge in surface hydrology. Runoff models must specify a resistance formulation or "roughness scheme"—describing the functional relationship between flow resistance and flow depth/velocity—and its parameters. Uncertainty in runoff predictions derives from both the selected roughness scheme (e.g., Darcy Weisbach, Manning's, or laminar flow equations), and its parameterization with a roughness coefficient (e.g., Manning's n). Both choices are informed by model calibration to data, usually discharge, and, if available, velocity. In this study, a Saint Venant Equation-based runoff model is calibrated to discharge and velocity data from 112 rainfall simulator experiments. The results are used to identify the optimal roughness scheme among four widely-used options for each experiment, and to explore whether surface properties can be used to select the optimal roughness scheme and its coefficient. Among the tested roughness schemes, a transitional flow equation provided the best fit to the plurality of experiments. The most suitable roughness scheme for a given experiment was not related to measured surface properties. Regression models predicted the calibrated roughness coefficients with adjusted r^2 values between 0.48 and 0.54, depending on the roughness scheme used. Litter cover was the best predictor of the roughness coefficient, followed by soil cover and average canopy gap size. The results suggest that selection of an optimal roughness scheme based on surface properties alone remains difficult, but that once a scheme is selected, roughness coefficients can be estimated from surface properties.

Plain Language Summary

Runoff prediction assists land and water management in drylands, but is challenging in part because of difficulties in specifying the "flow resistance" (frictional losses impeding water flow). Flow resistance is represented by a resistance equation, or "roughness scheme," which describes how resistance depends on the flow depth and velocity, and the land surface. Most roughness schemes represent the land surface roughness with a "roughness coefficient," (i.e., Manning's n). Reliably determining the best roughness scheme and its coefficient from rainfall and land surface data remains an unresolved challenge. The roughness scheme and its coefficient are usually determined by calibrating runoff models to discharge data. Unfortunately, multiple roughness schemes can be tuned to fit the same discharge data similarly well. Since the roughness scheme determines how velocity varies with discharge, some calibrated schemes may bias velocity predictions. Here, we calibrate a runoff model to 112 rainfall simulator experiments for which both discharge and velocity data were collected. We use the data set to compare four commonly-used roughness schemes. The results suggest that calibration using both discharge and velocity is valuable in selecting the best roughness scheme. For the best-fit scheme, the calibrated roughness coefficients vary with surface properties, particularly leaf litter cover.

1. Introduction

The partitioning of rainfall between infiltration and runoff at the land surface determines the hydrological behavior of dryland regions. These arid and semiarid regions comprise some 40% of the earth's surface and are characterized by sporadic rainfall that produces transient and shallow surface flows (Horton, 1933; Maestre et al., 2012; Reynolds et al., 2007). In dryland regions, runoff is a primary mechanism for the transport of water and nutrients from bare soil sources to vegetated sinks, augmenting plant water availability and sustaining vegetation in regions where direct rainfall inputs alone would be insufficient (Assouline et al., 2015; Okin et al., 2009; Schlesinger et al., 1990). Because ecosystem function and surface hydrology are tightly coupled,

Table 1

Summary of the Tested Roughness Schemes, Where r Is a General Resistance Parameter, $Fr = U(ghS_o)^{-1/2}$ *Is the Local Froude Number and* $\mathrm{Re} = Uh/\nu$ *Is the Local Reynolds Number*

Name	Froude number form	Conveyance form	References
Bed friction roughness schemes			
Darcy Weisbach	$Fr^2 = \frac{8}{f}$	$U = \frac{1}{r}h^{1/2}S_o^{1/2}$	Brutsaert (2005)
		$r = \sqrt{\frac{f}{8g}}, m = 1/2$	Cea et al. (2014)
Laminar	$Fr^2 = \frac{1}{K}\mathrm{Re}$	$U = \frac{1}{r}h^2 S_o$	Brutsaert (2005)
		$r = \frac{g}{K\nu}, m = 2$	Dunkerley (2003b)
Manning	$Fr^2 = \frac{h^{1/3}}{n^2 g}$	$U = \frac{1}{r}h^{2/3}S_o^{1/2}$	Brutsaert (2005)
		$r = n, m = 2/3$	Smith et al. (2007)
Mixed/Transitional	$Fr^2 = \frac{h}{r^2 g}$	$U = \frac{1}{r}hS_o^{1/2}$	Mügler et al. (2011)
		$r = T, m = 1$	Horton (1939)

Note. Other symbols are Manning's coefficient n, the Darcy Weisbach friction factor f (dimensionless), a roughness parameter for laminar flow K (Dunkerley, 2003b), the kinematic viscosity ν, and a roughness coefficient for transitional flow T (Brutsaert, 2005; Horton, 1939). The transitional formulation has the same functional form as the depth-dependent Manning's n trialed by Mügler et al. (2011). That is, r scales with $h^{1/3}$.

runoff prediction is necessary for any effort pertaining to ecological conservation, erosion control, drought mitigation and hazard response in drylands (Reynolds et al., 2007). For example, water erosion is often a significant driver of land degradation in dryland regions (Dregne, 2002), with erosion initiation tightly coupled to the velocity of runoff (Govers et al., 2007; Wu et al., 2017). Similarly, surface water is often required for drinking, irrigation, and livestock watering, meaning runoff prediction is necessary for water resources management (Rockstrom, 2000; Saha & Zeleke, 2015). At watershed scales, hydrologic models are needed for the implementation of real-time flood forecast and warning systems (Creutin & Borga, 2003; Kitanidis & Bras, 1980), and the implementation of proactive measures against flash floods.

The common equations with which to represent runoff from rainfall in dryland environments are the Saint Venant (or shallow water) equations (SVE). The SVE combine the continuity equation with conservation of momentum, and, in their one dimensional form, are expressed as:

$$\frac{\partial h}{\partial t} + \frac{\partial}{\partial x}(Uh) = (p - i), \tag{1}$$

$$\frac{\partial U}{\partial t} + U\frac{\partial U}{\partial x} + g\frac{\partial h}{\partial x} + g\left(S_f - S_o\right) = 0, \tag{2}$$

where h is the water depth at location x and time t, U is the depth-averaged velocity, g is the gravitational acceleration, S_o is the bed slope, and S_f is the friction slope, which represents the energy lost due to friction between the fluid and the surface. Precipitation p and infiltration i are forcing terms that can vary with position x and time t.

Because of S_f, the SVE do not form a closed system of equations, so a "closure" model in the form of a resistance formulation, hereafter a "roughness scheme," must be specified to represent the net effects of bed and other shear stresses on energy losses in the flow. Many roughness schemes exist, each describing the friction slope S_f in terms of modeled flow variables (i.e., h and U) and surface features. Table 1 summarizes four commonly-used roughness schemes. For a more in-depth discussion of these schemes, the work in Crompton et al. (2020) includes derivations of resistance formulations for bed and distributed drag. The four roughness schemes can be represented in dimensional form as:

$$U = r^{-1}h^m S_f^w, \tag{3}$$

where the exponents m and w link U to h and S_f, and the roughness coefficient r sets the magnitude of frictional resistance. Equation 3 provides closure to Equation 2 through the relation $S_f = \left(Urh^{-m}\right)^{1/w}$. A common choice

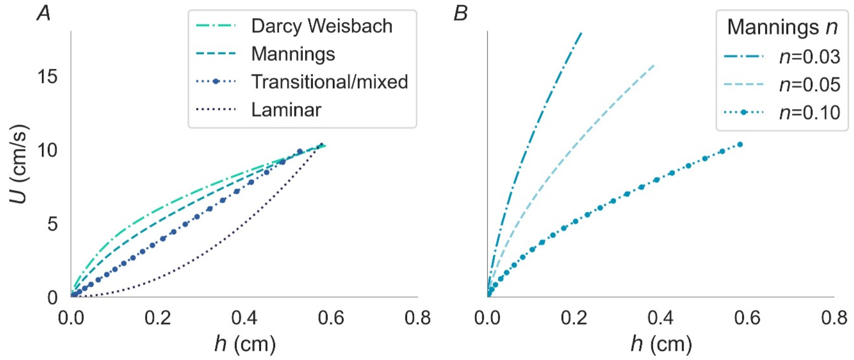

Figure 1. Illustration of the independent roles of the selection of a roughness scheme (m) and its parameterization (r) on the predicted relation between velocity U and depth h for a steady-state uniform flow. Under these conditions, the momentum equation simplifies to $S_f = S_o$ and Equation 3 simplifies to $U = r^{-1}h^m S_o^w$. Panel (a) illustrates how the selection of a roughness scheme implies a $U - h$ scaling relation for each roughness scheme, independent of the value of r (for each scheme, r has been adjusted to match flow properties between schemes at the outlet). Conversely, (b) illustrates model predictions for three values of Manning's n (with all other variables the same).

for S_f is Manning's equation for sheet flow, which can be written as $U = n^{-1}h^{2/3}S_f^{1/2}$. Here $m = 2/3$, $w = 1/2$ and $r = n$ or Manning's roughness, which is treated as a constant independent of the Reynolds number (Re $= Uh/\nu$, ν is the kinematic viscosity) in fully developed turbulent flows.

The parameterization of flow resistance thus entails both the selection of a roughness scheme to describe how U varies as a function of h and S_f, and the determination of a roughness coefficient, specific to both the chosen scheme and the land surface being represented. Determining the suitability of a roughness scheme for a given runoff problem is a longstanding challenge. For example, roughness schemes are often specified based on the nature of the flow being described. Yet overland flow can be laminar, turbulent, or transitional over very short distances depending on the bed slope and surface cover (Abrahams et al., 1986; Roels, 1984), and has been described as "mixed flow" by Horton (1945) and "composite flow" by Abrahams et al. (1986).

The Darcy-Weisbach and Manning equations are the most widely used empirical equations to close S_f in runoff and erosion models. These equations were originally developed for steady, uniform pipe and channel flows, where the water depth far exceeds the mean geometric height of roughness elements. However, these conditions are rarely encountered in overland flows (Smith et al., 2007). Other studies have suggested that surface runoff is better represented as laminar (Dunkerley, 2003b; Woolhiser et al., 1970), given the low bulk Reynolds numbers typical for rainfall runoff studies. Finally, in an intercomparison of four roughness schemes, Mügler et al. (2011) found that a transitional formulation of the form $U = r^{-1}hS_o^{1/2}$ provided the best fit to the velocity data (note that Mügler et al. (2011) label it a depth-dependent Manning's equation).

For modeling purposes, a uniform roughness coefficient is typically applied within the domain, and its value adjusted via calibration to reproduce the discharge observations (e.g., calibration of Manning's n to the runoff hydrograph). However, multiple roughness schemes can produce acceptable agreement with runoff measurements through calibration (Cea et al., 2014; Crompton et al., 2020; Mügler et al., 2011), posing equifinality as a challenge in selecting the most appropriate model. While this may not be problematic for discharge prediction per se, the roughness scheme determines how U varies as a function of h and S_f. Thus, model calibration to discharge may result in selection of a roughness scheme that biases velocity predictions.

This is illustrated in Figure 1a, which plots h versus U for four roughness schemes for the case of steady-state, uniform flow. Once a scheme is identified, the roughness coefficient plays an independent role in shaping the h versus U relationship, as is illustrated for the case of Manning's equation in Figure 1b. A solution to this problem is to incorporate both velocity and discharge data in runoff model calibration. However, such jointly-informed calibration is rarely performed (a notable exception is Mügler et al. (2011), who compared several roughness schemes using rainfall simulator experiments conducted in Senegal).

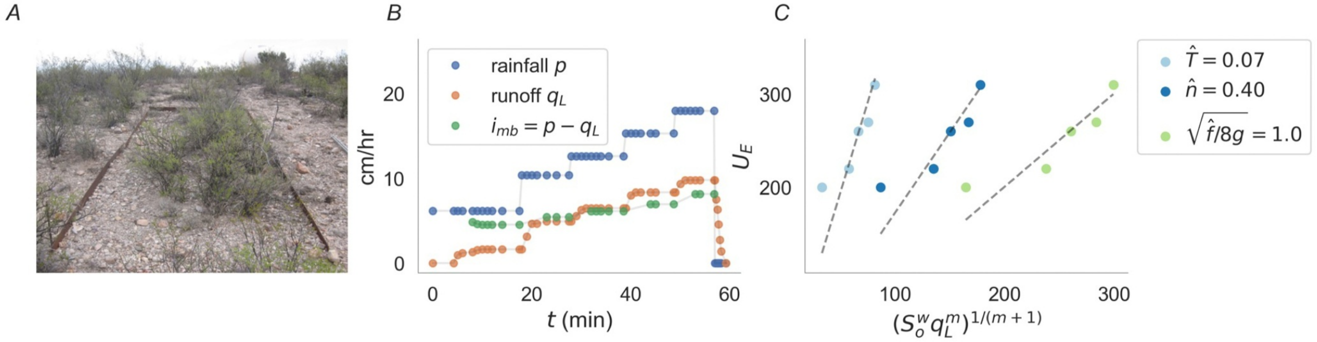

Figure 2. Panel (a) shows a sample plot selected from Lucky Hills in the Walnut Gulch Experimental Watershed, with dimensions 6 × 2 m. Panel (b) shows rainfall simulator data collected at the site, with infiltration rate i estimated as the difference between applied rainfall and collected runoff, $p - q_L$. Panel (c) illustrates—for the same experiment—how the experimental resistance r_E was estimated using linear regression of U_E on $\left(S_o^w q_L^m\right)^{1/(m+1)}$ for each experiment and roughness scheme. Note that the exponents m and w—and thus units in $\left(S_o^w q_L^m\right)^{1/(m+1)}$—differ between roughness schemes in Panel (c).

This study therefore uses a joint calibration approach incorporating discharge and velocity data, to evaluate the suitability of four commonly-used roughness schemes to model shallow, rain-driven overland flow. A public rainfall simulator data set (Polyakov et al., 2018) consisting of 112 rainfall simulator experiments conducted throughout the US Southwest, in which both discharge and velocity were measured for varying rainfall intensities (see Figure 2b), offers a unique opportunity for calibration to multiple experiments. Surface properties—including soil texture and vegetative, litter, rock, and bare soil cover—were surveyed prior to each experiment, providing a rich data set to evaluate the correspondence between surface properties and hydrodynamic roughness.

The experimental data set and model calibrations are used to address the following research questions (RQs):

1. Considering the 112 rainfall experiments together, which roughness scheme best fits this expansive data?
2. Anticipating that the "best" roughness scheme will vary between experiments, can surface properties be used to predict the suitability of a given roughness scheme to a given experiment?
3. Can the roughness coefficient of a selected roughness scheme be predicted from surface properties?

We address these questions by calibrating the model to each experiment and for each roughness scheme, using two approaches: firstly, by tuning the roughness coefficient to minimize the discharge prediction error (as conventionally done), and secondly, to minimize the velocity prediction error. We evaluate roughness scheme suitability using the criteria that the two approaches should yield the same (or similar) roughness coefficients and comparable calibration errors. To examine whether physical attributes of the land surface are predictive of scheme suitability, we label each experiment as successfully- or unsuccessfully-calibrated, and ask whether surface properties differ significantly between these groups. Research Question 3 is empirically addressed using regression and machine learning (ML) approaches to predict the calibrated roughness coefficients from the measured surface properties.

2. Methods

2.1. Rainfall Simulator Data Set

The data set is comprised of a series of 112 rainfall simulator experiments conducted on grass, shrub, oak savanna, and juniper sites in Arizona and Nevada, and is described elsewhere (Polyakov et al., 2018). The surface properties span a wide range of conditions, including a range of soil textures from clay loam to very gravelly loam. Rainfall was generated by the Walnut Gulch Rainfall Simulator, a portable variable-intensity simulator that can deliver rainfall rates p ranging between 13 and 178 mm/hr with a variability coefficient of 11% across a 6 × 2 m area (Paige et al., 2004). The data were collected between 2006 and 2013 on 20 rangeland sites, where each site contained between 4 and 12 replicate plots. The plots were constructed with sheet metal borders, and runoff was collected in a trough on the downslope side of each plot. To saturate the soil, the plots were subjected to a 45 min long pre-wetting at 65 mm h^{-1}.

In each experiment, the rainfall intensity was increased incrementally (see Figure 2 illustrating a sample runoff plot and collected data). For each rainfall intensity, velocity measurements were taken under steady-state conditions, with 4–6 measurements per experiment. The experimental velocity U_E was measured using the mean transit time obtained from electrolyte solution released from a perforated PVC pipe placed across each plot located 3.3 m from the outlet, and thus represents the spatial average velocity over the distance traveled by the electrolyte tracer (i.e., from $x = 2.7$ m to the outlet $x = 6$ m, where $x = 0$ at the upslope boundary). The runoff rate Q_E [L^3/T] from the plot was measured using a V-shaped supercritical flume positioned at a 4% slope and equipped with an electronic depth gauge. The experimental flow rate per unit width can be computed as $q_L = Q_E/b$ [L^2/T] where $b = 2$ m is the plot width. For a given roughness scheme, the experimental resistance r_E is defined as:

$$r_E = h_E^m S_f^w U_E^{-1}, \tag{4}$$

where h_E [L] is the experimental depth estimated as $h_E = q_L/U_E$. For example, for Manning's equation, $n_E = h_E^{2/3} S_o^{1/2} U_E^{-1}$. The computed values of r_E depend on the specified roughness scheme (i.e., Manning's n is not directly comparable to the Darcy Weisbach friction factor f).

Prior to each rainfall simulation, surface and vegetative cover were measured at 400 points on a 15 cm × 20 cm grid using a laser and line-point intercept procedure (Herrick, 2005). At each point, vegetative cover was classified as forbs, grass, and shrub, and the percent coverage was computed for each cover type. The surface cover was similarly classified at each point as rock, litter, plant basal area, and bare soil, and converted to percentages. These four metrics were further classified as protected (located under plant canopy) and unprotected (not covered by the canopy). Plant canopy gaps and basal gaps were measured on the plots over three lengthwise and six crosswise transects. These were reported as the average of all inter-canopy and inter-basal spaces greater than 10 cm along the transects.

2.2. The Saint Venant Equations Model

The rainfall simulator experiments were modeled using an open-source SVE model, FullSWOF (Delestre et al., 2014), that has been validated on a library of analytic solutions to the SVE (Delestre et al., 2013) and real rainfall events (Tatard et al., 2008). The friction slope S_f is specified by Equation 3, with exponents m and w listed in Table 1 and the coefficient r obtained through model calibration.

Infiltration in the model is computed at each cell using a modified Green Ampt equation. In its original form, the Green Ampt equation predicts the movement of water into the soil as an advancing wetting front separating a saturated zone from an underlying zone with initial soil moisture θ_i. At the timestep $t = t_n$, the soil infiltration capacity i_c^n [L/T] is given as:

$$i_c^n = K_s\left(1 + \frac{H}{I^n}\right), \tag{5}$$

where K_s is the saturated hydraulic conductivity (L/T), and I^n is the cumulative infiltration at timestep n, and $H = \psi_f(\theta_s - \theta_i)$ is a grouped parameter in which ψ_f is the wetting front capillary pressure head (L), $(\theta_s - \theta_i)$ is the moisture deficit, and θ_s is the saturated water content (approximating the soil porosity). The infiltration rate is then computed as: $i^n = \min(i_c, p + h/dt)$, where h is the local surface water depth.

Preliminary assessment of the data indicated that the rate of infiltration—estimated as the difference between rainfall and runoff—in some cases increased over the rainfall duration, which could indicate subcritical soil water repellency. Subcritical repellency has been reported for many natural and agricultural soils worldwide and has been attributed to water-solid contact angle exponentially decreasing in time (Wang & Wallach, 2021). To accommodate this effect in the current modeling framework, a correction factor proposed by Abou Najm et al. (2021) was incorporated, which adjusts the Green Ampt infiltration rate by a factor of $(1 - e^{-\alpha_R t})$:

$$i_c^n = K_s\left(1 + \frac{H}{I^n}\right)\left(1 - e^{-\alpha_R t}\right), \tag{6}$$

where α_R is a rate-constant parameter whose reciprocal reflects the time-scale of water repellency and thus characterizes the duration of water repellency. Smaller α_R represents greater repellency, and $\alpha_R = \infty$ for non-repellent soils.

2.3. Model Calibration

We calibrated the SVE model to each experiment and for each roughness scheme using a sequential approach in which: (a) the Green Ampt infiltration parameters were estimated, (b) the experimental resistance r_E was estimated from the measured U_E and q_L, and (c) the estimated infiltration and roughness parameters were used to set the ranges of parameter values tested in the SVE model simulations. Each of these steps is described in more detail below. Other boundary conditions—including the rainfall intensity p and slope gradient S_o—were provided directly by the experimental data.

(1) Infiltration parameters: The infiltration parameters—K_s, H and α_R—were estimated by fitting Equation 6 to the infiltration rate, which we estimated as the difference between rainfall intensity and discharge (filtered to omit periods of runoff adjustment following changes in rainfall intensity). Specifically, Equation 6 was solved using a gridded search approach, and the eight parameter combinations with the lowest root-mean squared errors were retained and tested in the SVE model simulations.

(2) Roughness estimation: The roughness coefficients were estimated by fitting a linear regression to Equation 4. Manning's n, for example, was estimated as the slope in $U_E = n_E^{-1} q_L^{2/5} S_o^{1/2}$. The goodness of fit was then computed as the normalized root mean square error (NRMSE):

$$\hat{E}(U_E, q_L) = \bar{U}_E^{-1} \sqrt{\frac{1}{N} \sum_i^N \left(U_{E,i} - \hat{U}_{E,i}\right)^2}, \tag{7}$$

where i indexes the velocity measurements, $\hat{U}_E$ is predicted from the linear regression equation, and $\bar{U}_E$ is the mean.

(3) SVE model calibration: For each roughness scheme, the SVE model was calibrated to each rainfall experiment using a gridded search approach, which included all combinations of the eight estimated soil parameter sets and 16 trialed values of r_E, ranging from $r_E/2$ to $2r_E$. Including the four trialed roughness schemes, 480 SVE model simulations were run for each rainfall simulator experiment, each model simulation requiring approximately 1 min to run. To calibrate the 112 experiments in the data set, $480 \times 112 = 53,760$ simulations were run in total.

For each rainfall simulator experiment and roughness scheme, the selection of eight parameter combinations in step (1) establishes a prior on the infiltration parameters, while the selection of 16 roughness coefficients in step (2) establishes a prior on the roughness parameters. These infiltration and roughness parameters are subsequently refined through the SVE model simulations.

2.4. Assessment Metrics Used to Quantify the Model Errors

Several objective functions were employed to assess the model prediction errors. The discharge error $E(q_L)$ is defined by the normalized root-mean squared error (NRMSE) between the measured and predicted q_L, and is given by:

$$E(q_L) = \bar{q}_L^{-1} \sqrt{\frac{1}{N} \sum_i^N \left(q_{L,i} - \hat{q}_{L,i}\right)^2}, \tag{8}$$

where $q_{L,i}$ and $\hat{q}_{L,i}$ are the measured and model-predicted runoff at timestep i, and $\bar{q}_L$ is the mean runoff used in the normalization. The velocity error $E(U_E)$ is similarly defined as:

Table 2
Error Metric and Roughness Coefficient Definitions

Symbol	Description
Error metrics	
$E(q_L)$	Hydrograph normalized root mean square error (Equation 8).
$E(U_E)$	Velocity normalized root mean square error (Equation 9).
B	Mean normalized velocity error (Equation 10).
Roughness coefficients	
r_E	Experimental resistance computed from observed discharge and velocity ($r_E = h_E^m S_f^w U_E^{-1}$).
r_U	Roughness calibrated by minimizing the velocity error, $E(U_E)$.
r_q	Roughness calibrated by minimizing the discharge error, $E(q_L)$.

$$E(U_E) = \bar{U}_E^{-1}\sqrt{\frac{1}{N}\sum_i^N\left(U_{E,i} - \hat{U}_{E,i}\right)^2}, \tag{9}$$

where $U_{E,i}$ and $\hat{U}_{E,i}$ indicate the measured and model-predicted velocities at timestep i ($\hat{U}_E$ is computed as the mean velocity between the tracer release point, located 3.3 m upslope of the outlet, and the outlet in the SVE model output). Lastly, a velocity bias metric B is defined as:

$$B = \sum_i^N\left(\hat{U}_{E,i} - U_{E,i}\right) / \sum_i^N\left(U_{E,i}\right), \tag{10}$$

where positive values of B indicate that the model overestimates the measured velocity.

We define r_U and r_q as the roughness coefficients that minimize $E(U_E)$ and $E(q_L)$, respectively. Recognizing that a range of roughness coefficients can produce an acceptable agreement to q_L, an ensemble approach was used to estimate r_q for each experiment: (a) the parameter set with the lowest $E(q_L)$ was selected as the "best" fit to the data, (b) all parameter sets for which $E(q_L)$ was within 5% of the minimum $E(q_L)$ were designated as the calibrated parameter ensemble, and (c) the mean and standard deviation of r_q were obtained from this ensemble. The same approach was used to obtain r_U for each experiment, using $E(U_E)$ to determine the calibrated parameter ensemble.

2.5. Research Question 1: Roughness Scheme Suitability

To evaluate roughness scheme suitability, we assessed whether the two calibration approaches yield approximately the same roughness coefficients (i.e., whether $r_U = r_q$). Specifically, we used the ratio r_U/r_q, where an $r_U/r_q < 1$ means that model calibration to discharge yields a larger roughness coefficient than calibration to velocity, biasing the model to overestimate velocity. Likewise, an $r_U/r_q > 1$ means that model calibration to discharge biases the model to underestimate velocity.

We then assessed whether calibrating the model to discharge yields accurate velocity predictions, and vice versa. Table 2 summarizes the error metrics used to evaluate and compare errors between calibration approaches and roughness schemes. Briefly, to evaluate the impact of different objective functions, we used subscripts to denote the calibration criteria:

- $E_q(q_L)$ is the discharge error obtained by calibrating the model to discharge (i.e., to minimize $E(q_L)$, which yields $r = r_q$).
- $E_U(q_L)$ is the discharge error obtained by calibrating the model to velocity (i.e., to minimize $E(U_E)$, which yields $r = r_U$).
- $E_q(U_E)$ is the velocity error obtained by calibrating the model to discharge ($r = r_q$).

- $E_U(U_E)$ is the velocity error obtained by calibrating the model to velocity ($r = r_U$).
- B_q is the velocity bias obtained by calibrating the model to discharge ($r = r_q$).
- B_U is the velocity bias obtained by calibrating the model to velocity ($r = r_U$).

These error metrics were compared between the four trialed roughness schemes, considering the ensemble of 112 rainfall simulator experiments together.

2.6. Research Question 2: Correspondence Between Surface Properties and Roughness Scheme Suitability

Research Question 2 asks whether surface properties—such as litter cover, soil texture, and slope gradient—can be used to predict the best roughness scheme for a given experiment. For each roughness scheme, we labeled each experiment as "successfully calibrated" if $0.8 < r_U/r_q < 1.2$, and "unsuccessfully calibrated" otherwise. This range of r_U/r_q coincides with low calibration errors (see Figure S2 in Supporting Information S1), so no additional criteria were used to classify experiments as successfully calibrated. "Successfully calibrated" is narrowly defined here to mean that calibration to discharge and calibration to velocity yield similar roughness coefficients. The experiments were labeled successfully- and unsuccessfully-calibrated to assess roughness scheme suitability, but the criterion of $0.8 < r_U/r_q < 1.2$ was not used to exclude experiments from the RQ 3 analysis (see Section 2.7). We did not set threshold goodness-of-fit criteria for $E(q_L)$, $E(U_E)$, or B, because the calibration errors largely depend on the infiltration—specifically, whether the modified Green Ampt model suitably describes the infiltration behavior.

The requirement that $0.8 < r_U/r_q < 1.2$ was met by exactly one scheme in 50 of the 112 rainfall simulator experiments, zero schemes in 38 experiments, two schemes in 18 experiments, and three schemes in 6 experiments. This range of r_U/r_q values maximizes the number of experiments for which exactly one roughness scheme is successfully calibrated. A more restrictive r_U/r_q range increases the number of experiments for which no experiments are labeled suitable. Conversely, a less restrictive range increases the number of experiments for which multiple roughness schemes are labeled suitable.

For each roughness scheme, we used the Kolmogorov-Smirnov test to assess whether any of the surface properties were significantly different between successfully and unsuccessfully calibrated groups. We also fit logistic regression models using surface properties to predict scheme suitability (i.e., whether an experiment is labeled as successfully-calibrated or not). Finally, we trialed various parametric and machine learning approaches to predict the calibration errors directly from surface properties.

While our primary aim is to evaluate the correspondence between surface properties and roughness scheme suitability, we also assessed whether measured flow characteristics, such as the bulk Reynolds and Froude numbers are predictive of roughness scheme suitability.

2.7. Research Question 3: Correspondence to Surface Properties

For each roughness scheme, we trialed several approaches to predict the calibrated roughness coefficients from the measured surface properties, including common parametric approaches (e.g., multivariate linear regression, power law, Gaussian, and exponential fits), and machine learning approaches (e.g., random forest regression, gradient boosting regression, k-nearest neighbors). Details of the machine learning approach are provided in the Supporting Information S1.

We did not include dynamic variables, such as the Reynolds and Froude numbers, because these variables can be used to directly estimate the roughness coefficient for a given scheme (e.g., e.g., $f = 1/Fr^2$). Experimentally-estimated and model-calibrated roughness coefficients are closely related, and using the former to predict the latter limits ability to generalize to new environments.

Several variable selection methods were tested, including forward and backward stepwise regression. For the parametric approaches, the model fit was evaluated using the adjusted coefficient of determination (r^2), which takes into account how many independent variables are added to a particular model. The machine learning model performance was evaluated using k-fold cross-validation, a re-sampling procedure used to evaluate ML models on limited data samples.

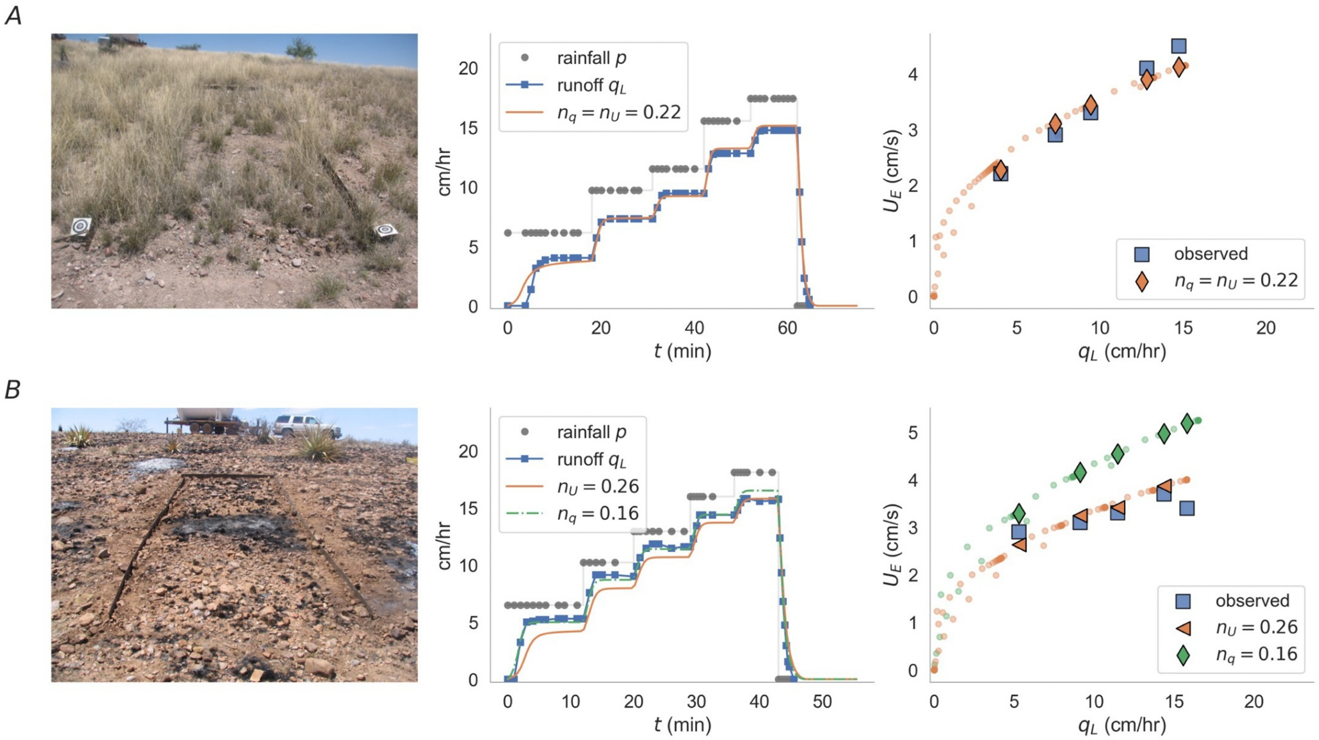

Figure 3. Sample results showing the model calibration for two rainfall simulator experiments with Manning's equation for flow resistance. In panel (a), calibration to discharge, q_L, yields the same roughness coefficient as calibration to velocity. In panel (b), calibration to velocity, U_E, yields a larger roughness coefficient than calibration to discharge. Note that, because Manning's n is used to parameterize flow resistance in these simulations, n_q and n_U are used in the legend instead of the more general r_q and r_U.

3. Results

Figure 3 illustrates the SVE model results for two example rainfall simulator experiments. Panel A shows an example in which model calibration to discharge yields the same roughness coefficient as calibration to velocity ($r_U = r_q$), and Panel B shows an example in which $r_U > r_q$. In Panel B, the hydrograph predicted using r_U is comparatively "sluggish" (compare blue and orange curves in the center panel), while the velocity predicted using r_q is overestimated (right panel).

For the Darcy Weisbach friction factor and Manning's roughness equations, the ranges of calibrated roughness coefficients are similar in magnitude to those reported in previous rainfall simulator studies (Emmett, 1970) (see the distributions of r_U and r_q in Figure 4a for each of the trialed roughness schemes). The range of calibrated laminar coefficients is also comparable to previous plot-scale studies (Dunkerley et al., 2001; Pan et al., 2016; Woolhiser et al., 1970). Of the surveyed studies, the only plot-scale study to include the transitional formulation reported $T = 0.089$ (Mügler et al., 2011), which is similar to the median calibrated roughness coefficients in the present study ($T_U = 0.056$ and $T_q = 0.054$) (Table 3).

3.1. Research Question 1: Roughness Scheme Comparison

Comparing the roughness coefficient distributions in Figure 4a, r_q and r_U most closely align for the transitional formulation ($m = 1$), followed by Manning's equation ($m = 2/3$). Figure 4b shows the distributions of r_U/r_q for each scheme. The median r_U/r_q is closest to one for the transitional formulation. For the Darcy Weisbach and Manning's equations, the median r_U/r_q is greater than one, and for laminar flow, the median r_U/r_q is less than one.

Violin plots in Figure 5 show the distributions of the discharge errors, $E_q(q_L)$ and $E_U(q_L)$ (panel a), velocity errors, $E_q(U_E)$ and $E_U(U_E)$ (panel b), and velocity biases, B_q and B_U (panel c). The left subplots show the errors obtained by calibration to discharge, and the right subplots show the errors obtained by calibration to velocity.

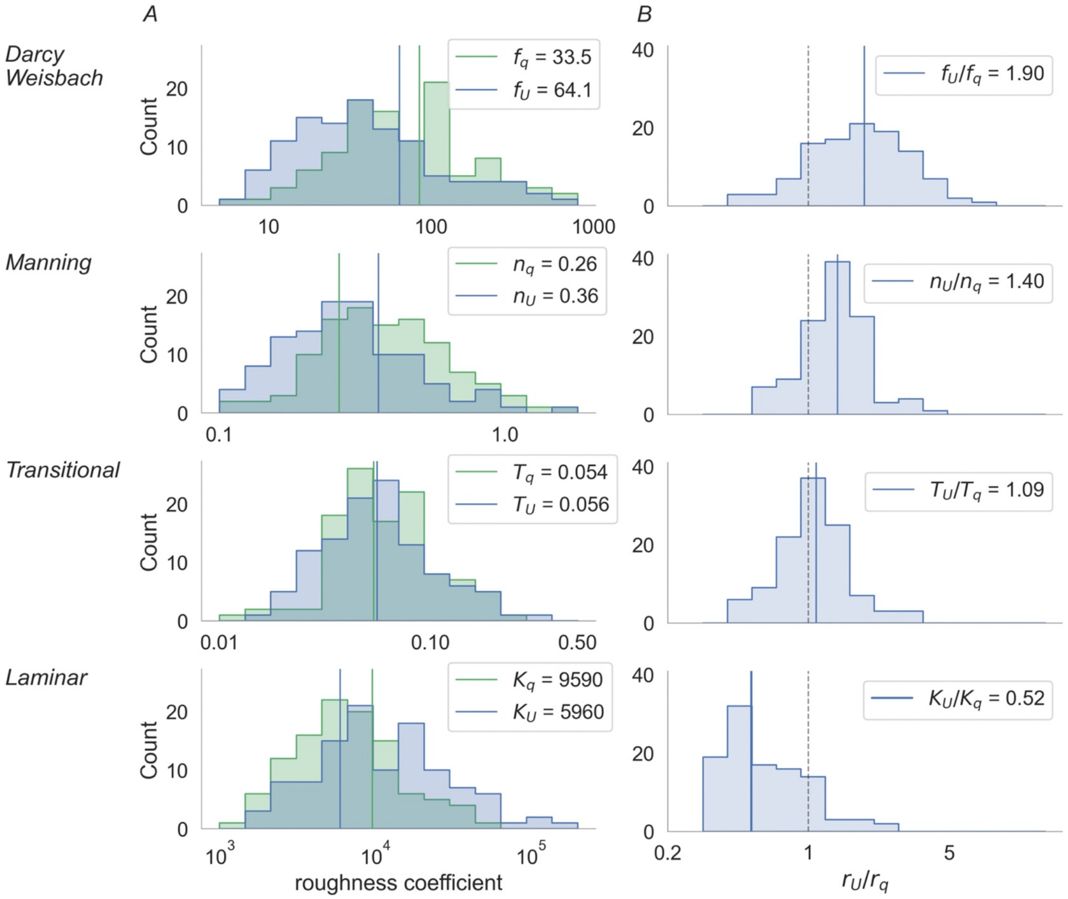

Figure 4. Panel (a) shows the distributions of roughness coefficients obtained through calibration to discharge (r_q, blue) and velocity (r_U, green) for each of the four roughness schemes. Vertical lines show the median values. Panel (b) shows the corresponding distributions of r_U/r_q, where values close to one indicate that the two calibration approaches yield consistent results.

Table 4 provides the median values and standard deviations for each error metric and scheme, summarizing the information in Figure 5. Visual inspection of the results indicated that cases with large calibration errors were, in most cases, those in which the modified Green Ampt model did not adequately describe the infiltration behavior (as determined from an imbalance between rainfall and discharge).

In Figure 5a, the distributions of $E_q(q_L)$ and $E_U(q_L)$ are similar across roughness schemes, echoing previous studies showing that multiple schemes can be calibrated to the same discharge data (Cea et al., 2014; Crompton et al., 2019; Mügler et al., 2011). Comparing left and right subplots in panel A, the two calibration approaches yielded comparable discharge errors. Specifically, the median $E_U(q_L)$ values are 30%–40% larger than the median $E_q(q_L)$ values. The velocity errors are more sensitive, both to the calibration approach and the roughness scheme. The median velocity errors are 2–4 times larger if the model is calibrated to discharge than if the model is calibrated to velocity (compare $E_q(U_E)$ and $E_U(U_E)$ in Figure 5b). The values of $E_q(U_E)$ are smaller for the transitional formulation than for the other roughness schemes, as are the differences between $E_q(U_E)$ and $E_U(U_E)$.

Table 3
Columns r_q and r_U Show the Median Roughness Coefficients Obtained Through Calibration to q_L and U_E, With Standard Deviations in Parentheses

	r_q	r_U	r_U/r_q
f	33.5 (98.2)	64.1 (173.2)	1.90 (2.52)
n	0.26 (0.21)	0.36 (0.25)	1.4 (0.55)
T	0.054 (0.05)	0.056 (0.044)	1.09 (0.52)
K	9590 (21188)	5960 (9109)	0.52 (0.41)

Note. Letters indicate the Darcy Weisbach equation (f, $m = 1/2$), Manning's equation (n, $m = 2/3$), transitional flow (T, $m = 1$) and laminar flow (K, $m = 2$). The ratio r_U/r_q is closest to unity for the transitional scheme.

The distributions of B_q in Figure 5c show that, for the Darcy Weisbach and Manning's equations, calibrating the model to discharge biases it to over-estimate velocity. For laminar flow, by contrast, calibrating the model to discharge biases it to underestimate velocity.

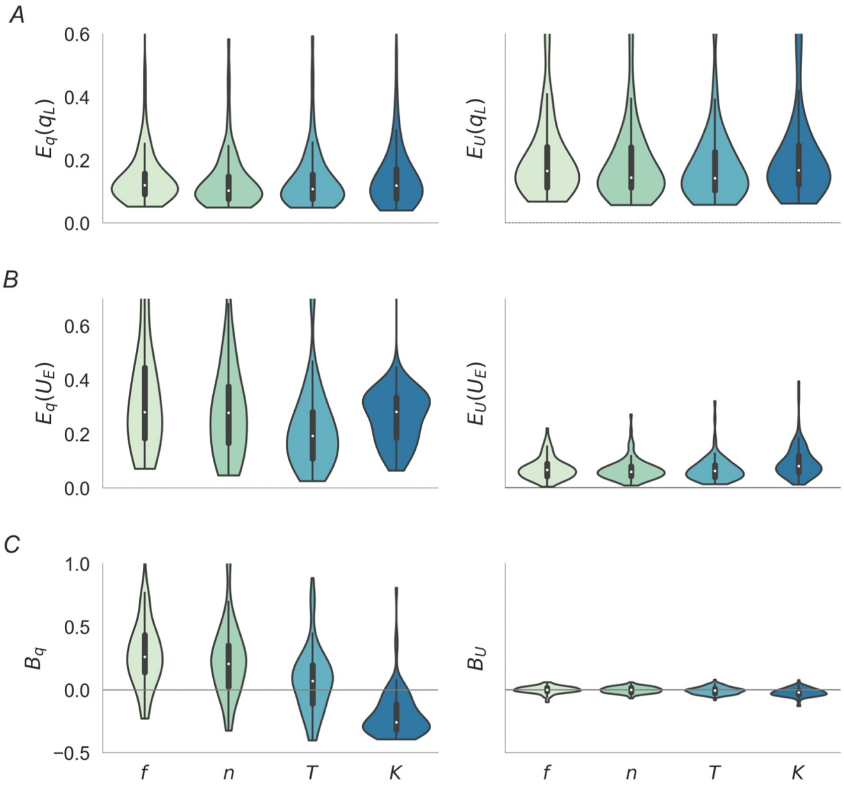

Figure 5. Violin plots show the distributions of discharge errors (E_q, panel a), velocity errors (E_U, panel b), and velocity bias (B, panel c). Letters indicate, from left to right: the Darcy Weisbach equation (f, $m = 1/2$), Manning's equation (n, $m = 2/3$), transitional flow (T, $m = 1$) and laminar flow (K, $m = 2$). The left subplots show the errors obtained through calibration to discharge, and the right subplots show the errors obtained through calibration to velocity. Comparing left and right subplots in panel (a), the discharge error is relatively insensitive to how the model is calibrated. In panels (b, c), by comparison, the velocity errors are generally much larger when the model is calibrated to discharge (left) than when it is calibrated to velocity (right).

For all schemes, small B_U values indicate, unsurprisingly, that calibration to velocity leads to unbiased velocity predictions. Across schemes, Figure 5 shows that calibration to discharge yields large velocity errors, while calibration to velocity yields modest discharge errors ($E_q(q_L) \approx E_U(q_L)$, while $E_q(U_E) > E_U(U_E)$). Thus, where possible, calibration using velocity data represents a more reliable approach.

3.2. Research Question 2: Can Surface Properties Predict the Best Roughness Scheme?

The criterion that $0.8 < r_U/r_q < 1.2$ was met by the transitional scheme in 42 experiments, Manning's equation in 27 experiments, the laminar equation in 17 experiments, and the Darcy Weisbach equation in 18 experiments. The Kolmogorov-Smirnov test revealed no significant differences in the measured surface properties between the

Table 4
Error Comparison Between Roughness Schemes

	$E_q(q_L)$	$E_U(q_L)$	$E_q(U_E)$	$E_U(U_E)$	B_q	B_U
f	0.12 (0.09)	0.17 (0.14)	0.28 (0.26)	0.07 (0.04)	0.27 (0.3)	0.0 (0.03)
n	0.12 (0.09)	0.15 (0.13)	0.27 (0.21)	0.06 (0.04)	0.2 (0.28)	0.0 (0.02)
T	0.11 (0.09)	0.15 (0.13)	0.19 (0.16)	0.06 (0.04)	0.07 (0.25)	−0.01 (0.03)
K	0.12 (0.11)	0.17 (0.15)	0.27 (0.11)	0.08 (0.06)	−0.23 (0.19)	−0.02 (0.03)

Note. Columns show median values, with standard deviations in parentheses. Letters indicate the Darcy Weisbach equation (f, $m = 1/2$), Manning's equation (n, $m = 2/3$), transitional flow (T, $m = 1$) and laminar flow (K, $m = 2$).

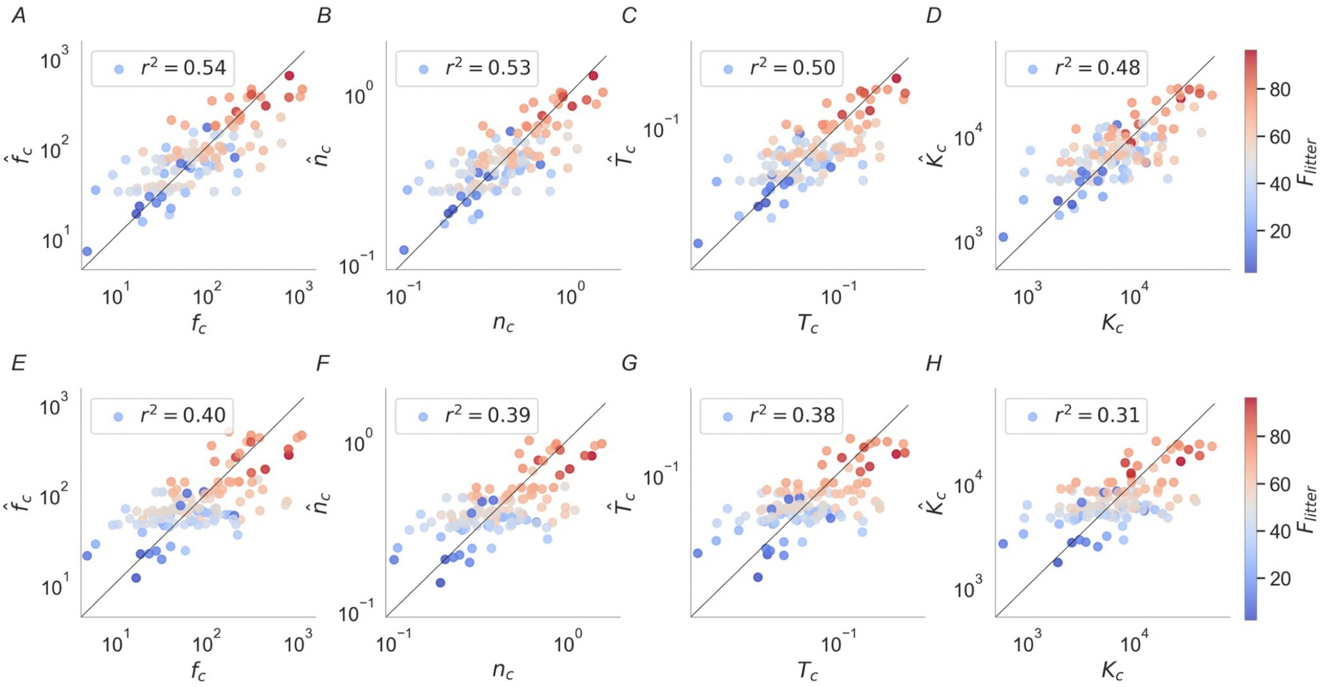

Figure 6. Equations for the power law fits to the roughness coefficients r_U for each roughness scheme on a double-log graph: (a) Darcy Weisbach, (b) Manning equation, (c) Transitional flow and (d) Laminar flow. The variables were selected with a backward selection method. Panels (e–h) show power law fits using the top three variables selected with stepwise forward selection (litter cover, soil cover and canopy gap size).

successfully- and unsuccessfully-calibrated experiments, for any of the roughness schemes (see Tables S2–S5 in Supporting Information S1). Additionally, no significant differences were detected in the bulk Reynolds or Froude numbers between the successfully- and unsuccessfully-calibrated experiments (see Tables S2–S5 in Supporting Information S1). Surprisingly, the laminar scheme did not outperform the other schemes in experiments with lower Reynolds numbers. This may, in part, be because the Re was low in all experiments ($\mathrm{Re} < 500$), such that there was limited scope to compare low and high Re cases. Moreover, the low Re here does not reflect the disturbed state of the flow due to rainfall splashing and random obstructions.

Alternative statistical approaches such as logistic regression also failed to predict scheme suitability. Lastly, parametric and machine learning regression approaches did not predict calibration errors with any accuracy.

3.3. Research Question 3: Correspondence Between Surface Properties and Calibrated Roughness Coefficients

Despite the insensitivity of roughness scheme suitability to surface properties, we now explore the correspondence between inferred roughness values and physical properties of the surface. Recall that the model calibration approach yielded two roughness coefficient versions: r_q, obtained by calibration to discharge, and r_U, obtained through calibration to velocity. Accordingly, we fit regression models to both r_q and r_U. The results are similar, both in terms of model accuracy and variable significance. This section presents the results for r_U, and the r_q results are included Figure S3 in Supporting Information S1 for completeness. Focusing on r_U is justified by the Research Question 1 result that calibration to velocity yields acceptable model accuracy for both U_E and q_L, while calibration to discharge yields large velocity errors.

The lowest errors were achieved using a power law function and backward feature selection (see scatter plots in Figure 6, panels a–d). With this approach, the Pearson correlation coefficients ranged from $r^2 = 0.48$ for the laminar scheme to $r^2 = 0.54$ for the Darcy Weisbach scheme. Thirteen variables were selected with backward feature selection: basal cover (protected and unprotected), canopy gap size, foliar cover (forb and total), ground cover (unprotected and total), litter cover (unprotected and total), rock cover (protected and unprotected), soil

Table 5
Power Law Fits to r_U Using the Top Three Variables Selected With Stepwise Forward Selection (Litter Cover F_{litter}, Soil Cover F_{soil}, and Average Canopy Gap Size $F_{canopy-gap}$)

	Equation	r^2
Darcy Weisbach	$f = 221.08\ F_{litter}^{0.43} F_{soil}^{-1.19} F_{canopy-gap}^{0.34}$	0.40
Mannings	$n = 0.68\ F_{litter}^{0.23} F_{soil}^{-0.58} F_{canopy-gap}^{0.14}$	0.39
Transitional	$T = 0.09\ F_{litter}^{0.33} F_{soil}^{-0.71} F_{canopy-gap}^{0.21}$	0.38
Laminar	$K = 13359.28\ F_{litter}^{0.31} F_{soil}^{-0.85} F_{canopy-gap}^{0.25}$	0.31

cover (protected), and slope. All variables have units of percent coverage, with the exceptions of slope and canopy gap size, as described in Section 2.1.

To simplify, we also fit a power law regression using the top three variables selected with forward variable selection, which were litter, soil cover, and canopy gap size (see Figure 6, Panels e–h, and Table 5). All variable selection methods found litter cover to be the best predictor of the calibrated roughness coefficients, followed by the total soil cover and canopy gap size.

Machine learning approaches yielded poorer fits to the data compared to other methods, as detailed Text S1 in Supporting Information S1. Among the tested models, gradient boosting regression provided the best results for the transitional formulation, Manning's equation, and laminar flow, with Pearson correlation coefficients (reported as the mean test-set r^2 from 5-fold cross-validation) ranging from $r^2 = 0.32$ for laminar flow to $r^2 = 0.38$ for the transitional formulation. The exception was the Darcy-Weisbach formulation, where k-nearest neighbors outperformed other models, with $r^2 = 0.32$. Figure S1 in Supporting Information S1 compares the r_U prediction errors using gradient boosting regression and k-nearest neighbors regression.

4. Discussion

The discharge errors were similar between the four trialed roughness schemes, and relatively insensitive to the calibration approach. This result is consistent with previous studies finding that multiple roughness schemes can be calibrated to fit the same discharge data. In particular, the studies of Mügler et al. (2011), Cea et al. (2014), and Crompton et al. (2020) demonstrated that multiple roughness schemes can produce acceptable agreement with runoff measurements through calibration.

The results show that discharge errors are similar between calibration approaches $\left(E_U\left(q_L\right) \approx E_q\left(q_L\right)\right)$. For instance, the median discharge errors are 30%–40% larger when the model is calibrated to velocity rather than discharge. Velocity errors, on the other hand, are two to four times greater when model calibration targets discharge versus velocity $(E_U(U_E) < E_q(U_E))$. This result is unsurprising, because velocity is more sensitive than discharge to the flow resistance parameterization. Unlike velocity, discharge more closely depends on factors controlling the volume of flow, namely, rainfall inputs and infiltration losses (i.e., the continuity equation). Notably, the discharge and velocity errors exhibit no significant correlation, suggesting that errors in the infiltration model do not affect the velocity errors.

Of the trialed roughness schemes, the transitional formulation provided the best overall fit to the experiments. The median $r_q/r_U \approx 1$ for the transitional scheme, suggesting that this formulation is most likely to provide unbiased predictions. This finding is consistent with the results of Mügler et al. (2011), which is the only previous rainfall simulator study to calibrate an SVE model to velocity measurements. Comparing four roughness schemes, Mügler et al. (2011) found that the data was best fit by a "depth-dependent" Manning's equation, that has the same $U \sim h$ scaling as the transitional scheme used here. However, whereas Mügler et al. (2011) calibrated an SVE model to a single plot, the present study included 112 rainfall experiments. The surface conditions in Mügler et al. (2011)—namely, bare, relatively impermeable soils—also differed from the plots modeled here, which had vegetation cover and exhibited complex infiltration behaviors.

Across the tested regression models, litter cover was the best predictor of the roughness coefficients. This finding is consistent with previous studies on flow resistance on dryland slopes (Abrahams et al., 1994; Al-Hamdan et al., 2013; Dunkerley, 2003a). Litter can reduce overland flow by inhibiting crust formation (Le Bissonnais et al., 1998; Puigdefábregas, 2005), and litter transported downslope may form micro-terraces that slow and spread overland flow (Ellis et al., 2006). Regression models predicting roughness coefficients from surface properties had limited success $\left(r^2 \approx 0.5\right)$, which may be attributable to the lumped nature of the measured surface properties. For example, the fractional cover of soil, litter, rocks, and vegetation elements represent average plot-scale statistics that do not capture potential for flow rivulets and meanders to form. Additionally, the power law fits to r_U and r_q may not generalize to other sites because the calibrated roughness coefficients likely depend on variables not considered in these experiments, such as domain size, microtopography, and the potential for concentrated flow paths to develop.

Model calibration to discharge resulted in similar discharge errors between schemes (i.e., similar distributions of $E_q(q_L)$), showing that jointly-informed calibration to discharge and velocity is needed to evaluate roughness scheme suitability. If velocity data is not available and the model is calibrated solely using discharge data—as is often the case—then the Darcy Weisbach and Manning's equations are biased toward underestimating the velocity, whereas the laminar formulation is biased toward overestimating it.

While the transitional roughness scheme is rarely implemented in runoff models (but see Jain et al., 2004; Rai et al., 2010), empirical studies often describe overland flow as mixed or transitional (Abrahams et al., 1986). However, no theoretical arguments have been offered to arrive at its form. In contrast to the other schemes in Table 1, the scaling relation between S_f, U and h does not conform to any prior boundary layer expectations. A novel and quantitative argument using a thermodynamic perspective is included in Appendix A, *A review of roughness schemes*.

Qualitatively, physical explanation for the transitional formulation may take advantage of spatial variability in both the horizontal and vertical dimensions. Horizontally, overland flow generally appears as a shallow sheet of water with threads of deeper, faster flow diverging and converging around surface obstructions, such as rocks and vegetation. If the flow is shallow but obstructed, there will be stagnation zones and fast flow regions along the horizontal paths, which may make the effective flow appear transitional along the entire flow path. As a result of these diverging and converging threads, flow depth and velocity may vary markedly over short distances, giving rise to a state of flow that has been labeled mixed or transitional (Abrahams et al., 1986; Horton, 1945).

In the vertical dimension, the transitional formulation can be framed as a depth-dependent Manning's n (Jain et al., 2004; Mügler et al., 2011; Rai et al., 2010), where the resistance decreases with increasing depth as the average submergence of soil surface roughness and vegetation elements increases. For flow over rough surfaces with obstructions such as pebbles or vegetation, the drag is large if the flow is shallow and sees the frontal area of the obstructions over the entire depth. Then, as the flow depth increases, the resistance decreases as the portion of the flow experiencing the frontal area decreases. Mathematically, the depth-dependent Manning's equation and spatially varying laminar/turbulent flow have the same functional form $\left(U = r^{-1}hS_o^{1/2}\right)$. Assessing which conceptual model better represents overland flow is beyond the study scope and is kept for a future inquiry.

The transitional roughness scheme provided the best calibration results to a plurality of experiments, but there were many cases in which a different scheme provided a better fit. We were not able to find any correspondence between surface properties and scheme suitability, despite being able to predict the calibrated roughness coefficients from surface properties with reasonable accuracy. This finding is not unexpected: unlike the roughness coefficient, which describes how rough a surface is, the roughness scheme specifies the "physics" of flow resistance. That is, the resistance formulation is intended to close the SVE by describing how velocity scales as a function of flow depth and S_f. The best choice of roughness scheme for a given surface likely depends on a number of subtle and interacting variables.

5. Conclusion

The study investigated the relation between surface properties and flow resistance in a data set consisting of 112 rainfall simulator experiments conducted in the US Southwest. Model calibration errors were compared among four commonly-used roughness schemes and two calibration approaches. To evaluate roughness scheme suitability, we first assessed whether calibration to discharge yields the same roughness coefficients as calibration to velocity. We then examined whether calibrating the model to discharge yields unbiased velocity estimates, and vice versa.

We found that all schemes perform equally well in predicting discharge, with relatively small sensitivity to how the model was calibrated. Conversely, model calibration to discharge may bias the velocity predictions if the selected roughness scheme is not suitable. In cases where jointly-informed calibration to velocity and discharge data is not possible, the transitional formulation appears to be the best a priori choice. However, the roughness coefficient associated with it lacks the rich history and literature values enjoyed by Manning's n and the Darcy-Weisbach f.

Appendix A: A Review of Roughness Schemes

The commonly-used resistance formulations in Table 1 can be represented in dimensionless form as:

$$\frac{U}{u_*} = \frac{U}{\sqrt{ghS_f}} = Fr = f_1\left(\frac{r_o}{h}, \mathrm{Re}\right), \tag{A11}$$

where $u_* = \sqrt{\tau_o/\rho}$ is the friction velocity, τ_o is the total frictional stress resisting the flow, ρ is the density of water, Fr is a Froude number, $\mathrm{Re} = Uh/\nu$ is a bulk Reynolds number, ν is the kinematic viscosity, r_o/h is a relative roughness, r_o is the absolute roughness. In the limit of high Re, f_1 depends only on r_o/h, as r_o far exceeds the viscous sublayer, whereas in the limit of very low Re, f_1 only depends on Re with r_o being entirely submerged within the viscous sublayer.

Equation 3 provides a mathematical closure to Equation 2 through the relation $S_f = (Urh^{-m})^{1/w}$. A case in point is Manning's equation for sheet flow, which can be written as $S_f = \left(Unh^{-2/3}\right)^2$. Here $m = 2/3$, $w = 1/2$ and $r = n$ where $n \sim r_o^{1/6}$ is Manning's roughness, which is treated as a constant independent of Re in fully developed turbulent flows (Bonetti et al., 2017).

As previously noted, roughness schemes must recover the idealized case where the flow is steady and uniform. For those conditions, the force balance between the gravitational forces driving the flow and the overall stresses τ_o opposing this motion leads to:

$$\tau_o/\rho = u_*^2 = ghS_o. \tag{A12}$$

For the quadratic drag law (i.e., $\tau_o = \rho C_d U^2$), the drag coefficient C_d relates the shear stress to U to yield:

$$C_d = \frac{u_*^2}{U^2} = \frac{f}{8}, \tag{A13}$$

where f is the Darcy-Weisbach friction factor. Combining Equations A12 and A13 yields the well-known Chezy formulation:

$$U = \frac{1}{\sqrt{C_d}}(ghS_o)^{1/2}. \tag{A14}$$

Equation A14 can be arranged so that:

$$\frac{U^2}{ghS_o} = Fr^2 = \frac{1}{C_d} = \frac{8}{f}. \tag{A15}$$

Hence, the particulars of a roughness scheme is reduced to describing C_d or f. For very low Re, the laminar formulation is recovered because

$$C_d = \frac{A_o}{Re} \text{ and } U = \frac{1}{A_o}\frac{g}{\mu}h^2 S_o, \tag{A16}$$

where A_o is a coefficient that depends on geometry. On the other hand, for very large Re, C_d is independent of Re and varies with the relative roughness r_o/h. That is:

$$C_d = A_1\left(\frac{r_o}{h}\right)^{m_1} \text{ and} \tag{A17}$$

$$U = \frac{1}{A_1}\left(\frac{h}{r_o}\right)^{m_1/2}(ghS_o)^{1/2}, \tag{A18}$$

where A_1 is also a proportionality coefficient. Manning's formula is recovered when $m_1 = 1/3$ (the Strickler scaling) whereas the empirical transitional formulation is recovered when $m_1 = 1$. These are the roughness schemes covered in Table 1 and are considered here.

The transitional scheme in Table 1 has been empirically proposed and included here given its previous success (Jain et al., 2004; Mügler et al., 2011). In contrast to the other schemes in Table 1, the scaling relation between C_d and $1/h$ does not conform to any prior boundary layer theory expectations. A number of conjectures may be offered as to why C_d scales with $1/h$ in such shallow overland flows. As h increases, some of the roughness obstacles "flip" from being emergent to being submerged and thus reduce the overall C_d. A variant on this argument is that with increased h, the flow resembles a continuous sheet thereby activating some of "dead-zones" (or stagnant water pools) in the domain. However, these arguments remain qualitative.

A thermodynamic argument is now offered. For steady uniform flow, the work per unit mass per unit time needed to move water at bulk velocity U is gS_oU. If this work is dissipated and converted into internal energy, then the bulk dissipation rate ϵ_b can be expressed as:

$$\epsilon_b = gS_oU = \frac{u_*^2}{h}U = C_d\frac{U^3}{h} = \frac{U^2}{\tau_d}, \tag{A19}$$

where $u_*^2 = ghS_o$ and τ_d is, by definition, a relaxation timescale. This τ_d can be interpreted as the time it takes to convert work (needed to move the water at U) into heat, and thus raise the internal energy of the water. From Equation A19,

$$\tau_d = \frac{1}{C_d}\frac{h}{U}. \tag{A20}$$

An intermediate case is now considered where the Re is sufficiently large so that wake production occurs. Such Re must be much larger than those associated with laminar flow (i.e., where $C_d = A_o/\mathrm{Re}$). However, the Re cannot be so large that the flow is fully turbulent and C_d is independent of Re. By fully turbulent, we mean there is a very large separation between turbulent production scales and the Kolmogorov micro-scales. For such very high Re values, wakes produced from obstacles cannot grow in space and are rapidly distorted or wiped out by turbulence, mainly through ejections and sweeps. Thus, the intermediate or transitional Re considered here are those associated with vortex production and subsequent growth (or shedding). Vortex shedding is initiated from the obstacle, leading to the periodic detachment of vortices that form what is known as a Kármán vortex street. To a leading order, Kármán vortex streets have a characteristic dissipation volume with three lengthscales: a horizontal length τ_dU, a width that scales with the obstacle diameter d_o, and a height that scales with the flow depth h. Hence, the shedding volume that the vortices occupy is τ_dUd_oh. However, for very shallow flows, where the most restrictive length is h, the dissipation of energy is occurring in many small spheres (or fine-scale eddies). During the cascade, the largest volume scales as τ_dUd_oh, and the smallest volume as h^3. If the energy cascade from large to small is volume-preserving or space-filling, then $\tau_dUd_oh \sim N_ch^3$, where N_c is the number of small-scale vortices produced just before viscous dissipation. Thus, we can set $\tau_dUd_oh = a_cN_ch^3$, where a_c is a proportionality coefficient. Combining this expression with Equation A20 yields:

$$C_d = \frac{h}{\tau_dU} = d_o(a_cN_ch)^{-1} \tag{A21}$$

Thus, C_d scales as h^{-1}, which is the sought result that recovers the transitional formulation.

Data Availability Statement

The data for this study were obtained from existing rainfall simulator experiments conducted in the U.S. Southwest (Polyakov et al., 2018). The data set is available from the National Agricultural Library at https://data.nal.usda.gov/search/type/dataset (https://doi.org/10.15482/USDA.ADC/1358583). FullSWOF is an open-source software distributed under CeCILL-V2 (GPL compatible) license and can be accessed at https://www.idpoisson.fr/en/fullswof/ (Delestre et al., 2014).

Acknowledgments
OC acknowledges funding from the National Science Foundation (NSF) Grant EAR-PF-1952651; and GK acknowledges support from NSF-AGS-2028644, and the U.S. Department of Energy (DE-SC0022072).

References

Abou, N. M. R., Stewart, R. D., Di Prima, S., & Lassabatere, L. (2021). A simple correction term to model infiltration in water-repellent soils. *Water Resources Research*, *57*(2), e2020WR028539. https://doi.org/10.1029/2020wr028539

Abrahams, A., Parsons, A., & Luk, S. H. (1986). Resistance to overland flow on desert hillslopes. *Journal of Hydrology*, *88*(3–4), 343–363. https://doi.org/10.1016/0022-1694(86)90099-5

Abrahams, A. D., Parsons, A. J., & Wainwright, J. (1994). Resistance to overland flow on semiarid grassland and shrubland hillslopes, walnut gulch, southern Arizona. *Journal of Hydrology*, *156*(1–4), 431–446. https://doi.org/10.1016/0022-1694(94)90088-4

Al-Hamdan, O. Z., Pierson, F. B., Nearing, M. A., Williams, C. J., Stone, J. J., Kormos, P. R., et al. (2013). Risk assessment of erosion from concentrated flow on rangelands using overland flow distribution and shear stress partitioning. *Transactions of the ASABE*, *56*(2), 539–548. https://doi.org/10.13031/2013.42684

Assouline, S., Thompson, S., Chen, L., Svoray, T., Sela, S., & Katul, G. (2015). The dual role of soil crusts in desertification. *Journal of Geophysical Research: Biogeosciences*, *120*(10), 2108–2119. https://doi.org/10.1002/2015jg003185

Bonetti, S., Manoli, G., Manes, C., Porporato, A., & Katul, G. G. (2017). Manning's formula and Strickler's scaling explained by a co-spectral budget model. *Journal of Fluid Mechanics*, *812*, 1189–1212. https://doi.org/10.1017/jfm.2016.863

Brutsaert, W. (2005). *Hydrology: An introduction*. Cambridge University Press.

Cea, L., Legout, C., Darboux, F., Esteves, M., & Nord, G. (2014). Experimental validation of a 2D overland flow model using high resolution water depth and velocity data. *Journal of Hydrology*, *513*, 142–153. https://doi.org/10.1016/j.jhydrol.2014.03.052

Creutin, J. D., & Borga, M. (2003). Radar hydrology modifies the monitoring of flash-flood hazard. *Hydrological Processes*, *17*(7), 1453–1456. https://doi.org/10.1002/hyp.5122

Crompton, O., Katul, G. G., & Thompson, S. (2020). Resistance formulations in shallow overland flow along a hillslope covered with patchy vegetation. *Water Resources Research*, *56*(5), e2020WR027194. https://doi.org/10.1029/2020wr027194

Crompton, O., Sytsma, A., & Thompson, S. (2019). Emulation of the Saint Venant equations enables rapid and accurate predictions of infiltration and overland flow velocity on spatially heterogeneous surfaces. *Water Resources Research*, *55*(8), 7108–7129. https://doi.org/10.1029/2019wr025146

Delestre, O., Cordier, S., Darboux, F., Du, M., James, F., Laguerre, C., et al. (2014). Fullswof: A software for overland flow simulation. In *Advances in hydroinformatics* (pp. 221–231). Springer.

Delestre, O., Lucas, C., Ksinant, P. A., Darboux, F., Laguerre, C., Vo, T. N. T., et al. (2013). Swashes: A compilation of shallow water analytic solutions for hydraulic and environmental studies. *International Journal for Numerical Methods in Fluids*, *72*(3), 269–300. https://doi.org/10.1002/fld.3741

Dregne, H. E. (2002). Land degradation in the drylands. *Arid Land Research and Management*, *16*(2), 99–132. https://doi.org/10.1080/153249802317304422

Dunkerley, D. (2003a). Organic litter: Dominance over stones as a source of interrill flow roughness on low-gradient desert slopes at fowlers gap, arid western NSW, Australia. *Earth Surface Processes and Landforms: The Journal of the British Geomorphological Research Group*, *28*(1), 15–29. https://doi.org/10.1002/esp.415

Dunkerley, D., Domelow, P., & Tooth, D. (2001). Frictional retardation of laminar flow by plant litter and surface stones on dryland surfaces: A laboratory study. *Water Resources Research*, *37*(5), 1417–1423. https://doi.org/10.1029/2000wr900399

Dunkerley, D. L. (2003b). Determining friction coefficients for interrill flows: The significance of flow filaments and backwater effects. *Earth Surface Processes and Landforms: The Journal of the British Geomorphological Research Group*, *28*(5), 475–491. https://doi.org/10.1002/esp.453

Ellis, T. W., Leguédois, S., Hairsine, P. B., & Tongway, D. J. (2006). Capture of overland flow by a tree belt on a pastured hillslope in south-eastern Australia. *Soil Research*, *44*(2), 117–125. https://doi.org/10.1071/sr05130

Emmett, W. W. (1970). *The hydraulics of overland flow on hillslopes* (Vol. 662). US Government Printing Office.

Govers, G., Giménez, R., & Van Oost, K. (2007). Rill erosion: Exploring the relationship between experiments, modelling and field observations. *Earth-Science Reviews*, *84*(3–4), 87–102. https://doi.org/10.1016/j.earscirev.2007.06.001

Herrick, J. E. (2005). *Monitoring manual for grassland, Shrubland and savanna ecosystems* (Vol. 2). University of Arizona Press.

Horton, R. E. (1933). The role of infiltration in the hydrologic cycle. *Eos, Transactions American Geophysical Union*, *14*(1), 446–460.

Horton, R. E. (1939). The interpretation and application of runoff plat experiments with reference to soil erosion problems. *Soil Science Society of America Journal*, *3*(C), 340–349. https://doi.org/10.2136/sssaj1939.036159950003000c0066x

Horton, R. E. (1945). Erosional development of streams and their drainage basins; hydrophysical approach to quantitative morphology. *Geological Society of America Bulletin*, *56*(3), 275–370. https://doi.org/10.1130/0016-7606(1945)56[275:edosat]2.0.co;2

Jain, M. K., Kothyari, U. C., & Raju, K. G. R. (2004). A gis based distributed rainfall–runoff model. *Journal of Hydrology*, *299*(1–2), 107–135. https://doi.org/10.1016/j.jhydrol.2004.04.024

Kitanidis, P. K., & Bras, R. L. (1980). Real-time forecasting with a conceptual hydrologic model: 1. Analysis of uncertainty. *Water Resources Research*, *16*(6), 1025–1033. https://doi.org/10.1029/wr016i006p01025

Le Bissonnais, Y., Benkhadra, H., Chaplot, V., Fox, D., King, D., & Daroussin, J. (1998). Crusting, runoff and sheet erosion on silty loamy soils at various scales and upscaling from m2 to small catchments. *Soil and Tillage Research*, *46*(1–2), 69–80. https://doi.org/10.1016/s0167-1987(98)80109-8

Maestre, F. T., Salguero-Gomez, R., & Quero, J. L. (2012). It is getting hotter in here: Determining and projecting the impacts of global environmental change on drylands. *Philosophical Transactions of the Royal Society B: Biological Sciences*, *367*(1606), 3062–3075. https://doi.org/10.1098/rstb.2011.0323

Mügler, C., Planchon, O., Patin, J., Weill, S., Silvera, N., Richard, P., & Mouche, E. (2011). Comparison of roughness models to simulate overland flow and tracer transport experiments under simulated rainfall at plot scale. *Journal of Hydrology*, *402*(1–2), 25–40. https://doi.org/10.1016/j.jhydrol.2011.02.032

Okin, G. S., Parsons, A. J., Wainwright, J., Herrick, J. E., Bestelmeyer, B. T., Peters, D. C., & Fredrickson, E. L. (2009). Do changes in connectivity explain desertification? *BioScience*, *59*(3), 237–244. https://doi.org/10.1525/bio.2009.59.3.8

Paige, G. B., Stone, J. J., Smith, J. R., & Kennedy, J. R. (2004). The walnut gulch rainfall simulator: A computer-controlled variable intensity rainfall simulator. *Applied Engineering in Agriculture*, *20*(1), 25–31. https://doi.org/10.13031/2013.15691

Pan, C., Ma, L., Wainwright, J., & Shangguan, Z. (2016). Overland flow resistances on varying slope gradients and partitioning on grassed slopes under simulated rainfall. *Water Resources Research*, *52*(4), 2490–2512. https://doi.org/10.1002/2015wr018035

Polyakov, V., Stone, J., Holifield Collins, C., Nearing, M. A., Paige, G., Buono, J., & Gomez-Pond, R. L. (2018). Rainfall simulation experiments in the southwestern USA using the walnut gulch rainfall simulator. *Earth System Science Data*, *10*(1), 19–26. https://doi.org/10.5194/essd-10-19-2018

Puigdefábregas, J. (2005). The role of vegetation patterns in structuring runoff and sediment fluxes in drylands. *Earth Surface Processes and Landforms: The Journal of the British Geomorphological Research Group*, *30*(2), 133–147. https://doi.org/10.1002/esp.1181

Rai, R., Upadhyay, A., & Singh, V. (2010). Effect of variable roughness on runoff. *Journal of Hydrology*, *382*(1–4), 115–127. https://doi.org/10.1016/j.jhydrol.2009.12.022

Reynolds, J. F., Smith, D. M. S., Lambin, E. F., Turner, B., Mortimore, M., Batterbury, S. P., et al. (2007). Global desertification: Building a science for dryland development. *Science*, *316*(5826), 847–851. https://doi.org/10.1126/science.1131634

Rockstrom, J. (2000). Water resources management in smallholder farms in eastern and southern africa: An overview. *Physics and Chemistry of the Earth - Part B: Hydrology, Oceans and Atmosphere*, *25*(3), 275–283. https://doi.org/10.1016/s1464-1909(00)00015-0

Roels, J. (1984). Flow resistance in concentrated overland flow on rough slope surfaces. *Earth Surface Processes and Landforms*, *9*(6), 541–551. https://doi.org/10.1002/esp.3290090608

Saha, P. P., & Zeleke, K. (2015). Rainfall-runoff modelling for sustainable water resources management: Swat model review in Australia. *Sustainability of Integrated Water Resources Management: Water Governance, Climate and Ecohydrology*, 563–578. https://doi.org/10.1007/978-3-319-12194-9_29

Schlesinger, W. H., Reynolds, J. F., Cunningham, G. L., Huenneke, L. F., Jarrell, W. M., Virginia, R. A., & Whitford, W. G. (1990). Biological feedbacks in global desertification. *Science*, *247*(4946), 1043–1048. https://doi.org/10.1126/science.247.4946.1043

Smith, M. W., Cox, N. J., & Bracken, L. J. (2007). Applying flow resistance equations to overland flows. *Progress in Physical Geography*, *31*(4), 363–387. https://doi.org/10.1177/0309133307081289

Tatard, L., Planchon, O., Wainwright, J., Nord, G., Favis-Mortlock, D., Silvera, N., et al. (2008). Measurement and modelling of high-resolution flow-velocity data under simulated rainfall on a low-slope sandy soil. *Journal of Hydrology*, *348*(1–2), 1–12. https://doi.org/10.1016/j.jhydrol.2007.07.016

Wang, Z., & Wallach, R. (2021). Water infiltration into subcritical water-repellent soils with time-dependent contact angle. *Journal of Hydrology*, *595*, 126044. https://doi.org/10.1016/j.jhydrol.2021.126044

Woolhiser, D., Hanson, C., & Kuhlman, A. (1970). Overland flow on rangeland watersheds. *Journal of Hydrology (New Zealand)*, 336–356.

Wu, B., Wang, Z., Zhang, Q., Shen, N., & Liu, J. (2017). Modelling sheet erosion on steep slopes in the loess region of China. *Journal of Hydrology*, *553*, 549–558. https://doi.org/10.1016/j.jhydrol.2017.07.017